

Supporting Information

Enabling economic and safe anode pre-lithiation with high value-added material production via vacuum thermal reduction

*Yu-Ke Wang, Jia Lu, Wang-Qi Dai, Xin-Yu Cheng, Huan-Hao Lei, Jin-Ning Zuo, Hui-Kang Xia, Zheng-Wen Fu**

Shanghai Key Laboratory of Molecular Catalysis and Innovative Materials, Department of Chemistry, Fudan University, Shanghai, 200433, China.

* Corresponding author: zwfu@fudan.edu.cn (Zheng-Wen Fu).

Experimental Procedures

1. Chemicals

Firstly, lithium hydroxide $\text{LiOH}\cdot\text{H}_2\text{O}$ (99.98%, Aladdin) was heated at 200 °C for 1 hour to prepare anhydrous LiOH. Then, Ti (99.99%, Aladdin) and LiOH powder were planetary milled at a speed of 400 rpm for 2 hours in molar ratios of 1:2, 1:2.9, and 1:4 to obtain Ti-LiOH mixtures. Finally, these mixtures were compressed using a tablet press under 10 MPa to obtain the reaction reagents.

2. Vacuum thermal reduction (VTR) process

The reduction and evaporation process of lithium was carried out in a vacuum thermal evaporation device, ~1.0 g Ti-LiOH reagent was placed into the resistance crucible, the heating power was controlled by adjusting the input electric current, and the heating temperature was measured by K-type thermocouple (0~1300 °C), the chamber pressure was monitored by resistance gauge (ZJ-52T, ZHVAC, China) and ionization gauge (ZJ-27, ZHVAC, China), quartz crystal sensor (QI8010 6 MHz, Fil-Tech Inc, USA) was used to measure the deposition rate of lithium metal, and the total deposition thickness was determined by the integration of deposition rate with time. To prepare Li@Cu and Si/C-Li electrode, Copper foil and Si/C electrode were placed on the top of the chamber facing the evaporation source at a distance of 40 cm. The evaporation chamber was cooled down by flowing cold water (~10°C) to keep the temperature of the copper foil and electrode below 80 °C. The deposition process can be controlled by a rotary shield. When the desired thickness was achieved, Li@Cu and Si/C-Li electrode were cooled down for 20 min before being removed from the vacuum chamber. The electrodes were immediately transferred into the Ar-filled glovebox ($\text{O}_2 < 0.1$ ppm, $\text{H}_2\text{O} < 0.1$ ppm). All operations were carried out in a dry room with a dew point below -40 °C.

3. Post treatment of reduction residues

The reduction residues of Ti-LiOH mixtures were removed from the vacuum chamber until the temperature was below 80 °C. The reduction residues were planetary ball milled for 1 hour at 400 rpm, then the products were placed into a tube furnace and annealed at 850 °C for 2 hours in air, LiTi_2O_4 , $\text{Li}_4\text{Ti}_5\text{O}_{12}$ and Li_2TiO_3 powders were

synthesized by annealing reduction products with different Li/Ti element ratios. The pre-lithiation of Si/C (Si/C-Li) electrode was achieved by the spontaneous solid-state electrochemical corrosion reaction between Si/C active materials and the as-deposited lithium metal film (1.6 μm in thickness), the whole pre-lithiation reaction was completed in an Ar-filled glovebox ($\text{O}_2 < 0.1$ ppm, $\text{H}_2\text{O} < 0.1$ ppm).

4. Characterization methods

The morphological features of reduction products, as-synthesized $\text{Li}_4\text{Ti}_5\text{O}_{12}$ powder, as-deposited lithium metal film, Si/C and Si/C-Li electrode were observed by a scanning electron microscope (SEM, Regulus 8100, Hitachi) with an energy dispersive spectroscopy (EDS) detector and an optical microscope (GP-660 V). X-ray diffractometer (XRD, Bruker D8 Advance) was used to identify the phases of reduction products and products after annealing treatment. The surface chemistry of reduction products, as-synthesized $\text{Li}_4\text{Ti}_5\text{O}_{12}$, as-deposited lithium metal film, Si/C and Si/C-Li electrode were analyzed by X-ray photoelectron spectroscopy (XPS, PHI-5000 VersaProbe III). The mass fractions of Li and Ti elements in the reduction products were obtained by inductively coupled plasma-optical emission spectroscopy (ICP-OES, Avio 200). The high-resolution transmission electron microscopy (HR-TEM) images of as-synthesized $\text{Li}_4\text{Ti}_5\text{O}_{12}$ were observed using FEI Tecnai F20 instrument.

5. Cell assembly and electrochemical measurements

To prepare Si/C electrode, 90 wt.% Si/C active material powder, 5 wt.% Super P, and 5 wt.% sodium alginate were homogenized with water to form the uniform cast slurry, the slurry was cast onto a Cu foil and then blast dried at 60 $^\circ\text{C}$ for 12 hours, the as-obtained Si/C electrode was hollowed out to a size of $\Phi 14$ mm with 5.7 mg/cm^2 active material mass loading. LiCoO_2 electrode was prepared by the slurry of 90 wt.% LiCoO_2 active material and 5 wt.% Super P and 5 wt.% PVDF and N-methyl pyrrolidone (NMP) solvent, the slurry was cast onto a carbon-coated Al foil and then blast dried at 60 $^\circ\text{C}$ for 12 hours, the as-obtained LiCoO_2 electrode was hollowed out to a size of $\Phi 12$ mm with 11.2 mg/cm^2 active material mass loading. To fabricate $\text{Li}_4\text{Ti}_5\text{O}_{12}$ electrode, the as-prepared $\text{Li}_4\text{Ti}_5\text{O}_{12}$ powder and Super P were mixed in a mass ratio of 8:1 and planetary ball milled for 5 min at 400 rpm, then 10 wt.% PVDF

was added into the mixture with NMP solvent to prepare a uniform cast slurry, this slurry was casted onto Cu foils and blast dried at 60 °C for 12 h. The as-prepared electrode was hollowed out to a size of $\Phi 12$ mm with 1.6 mg/cm² active material mass loading. Both half and full cells were assembled with CR2032 type battery cases. The electrolyte was 1 mol/L LiPF₆ in ethylene carbonate (EC), ethyl methyl carbonate (EMC) and dimethyl carbonate (DMC) (v/v/v = 1:1:1) with 10% fluoroethylene carbonate (FEC). PE (16 μ m in thickness) base membrane coated with double-face Al₂O₃ ceramic layers (2 μ m in thickness) was used as the separator. Metallic lithium foil was employed as a counter/ reference electrode for the half cell. As for the full cell, the areal capacity ratio of anode/cathode (n/p) was controlled to be ~ 1.17 . The whole battery assembly procedures were operated in an Ar-filled glovebox (O₂<0.1 ppm, H₂O<0.1 ppm).

The charge/discharge performances of half and full cells were tested by CT-4008 battery testers (Neware, China) at 25 °C. The initial activation currents were 0.05C for Si/C half and full cells and 0.1C for Li₄Ti₅O₁₂ and LiCoO₂ half cells, the operating voltage ranges of Si/C, Li₄Ti₅O₁₂ and LiCoO₂ half cells were 0.01~1.5 V, 1.0~2.5 V and 3.0~4.5 V, respectively. The initial specific charge capacity of full cell was restricted below 215 mAh/g, corresponding to ~ 4.47 V cut-off voltage, and the subsequent operating voltage ranges of full cell was 3.0~4.45 V. Cyclic voltammetry (CV) measurements were carried out with a voltage scan rate of 0.1 mV/s at the CHI660e (Shanghai Chenhua, China) electrochemical workstation. The electrochemical impedance spectroscopy (EIS) was measured by Zennium pro (Zahner, Germany) electrochemical workstation between 1 MHz~10 mHz with an amplitude of 5 mV. The as-obtained EIS data were processed using the DRTtools software¹, the following values of the main parameters were used: method of discretization: Gaussian; regularization derivative: first-order; regularization parameter: 0.001; RBF shape control: shape factor; FWHM control: 1.5.

Results and Discussion

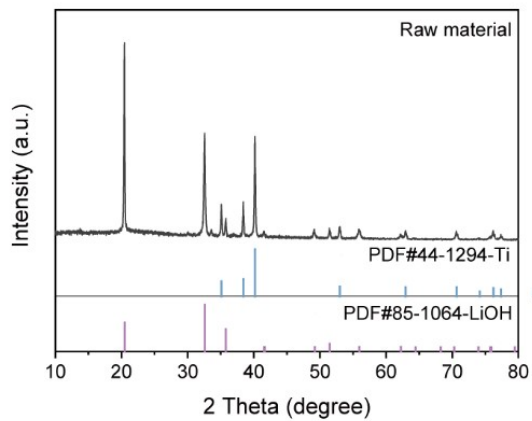


Figure S1. XRD pattern of Ti and LiOH mixtures.

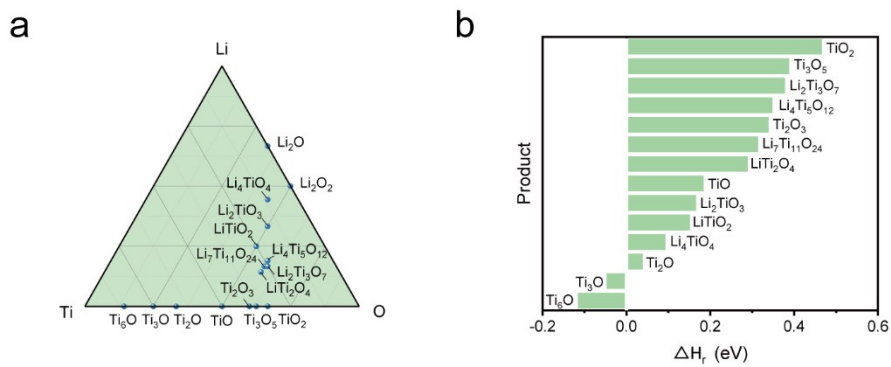


Figure S2. a) The phase equilibrium diagram of Li-Ti-O system². b) The products and corresponding thermodynamic enthalpy changes (ΔH_r) of the reaction between Ti and Li_2O^3 .

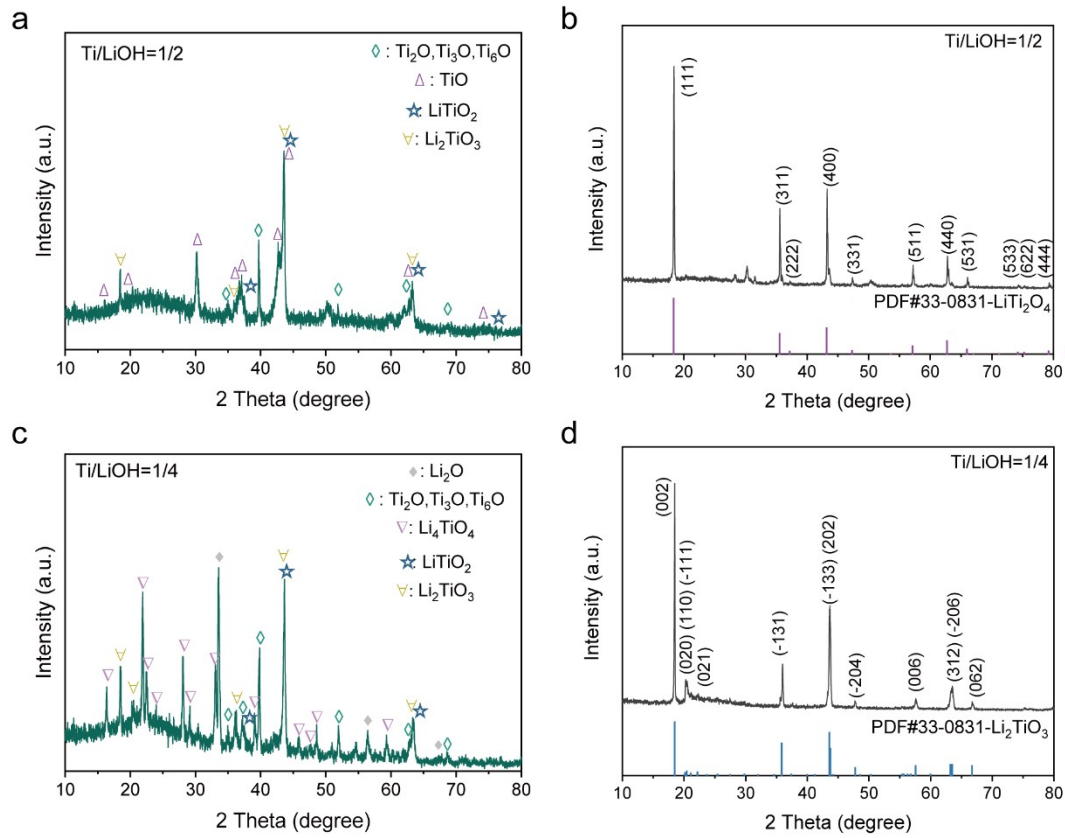


Figure S3. XRD patterns of reduction residues when the mole ratios of Ti/LiOH in raw materials are a) 1/2 and c) 1/4. XRD patterns of reduction residues after upcycling process: b) LiTi_2O_4 , d) Li_2TiO_3 .

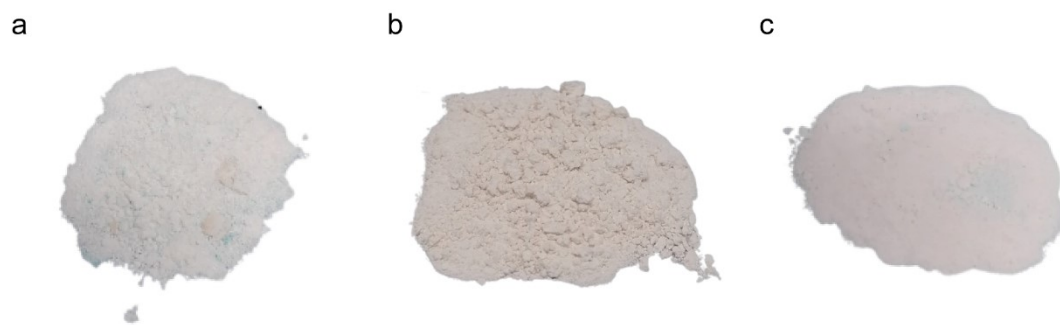


Figure S4. Optical images of reduction residues after annealing: a) LiTi_2O_4 , b) $\text{Li}_4\text{Ti}_5\text{O}_{12}$, c) Li_2TiO_3 .

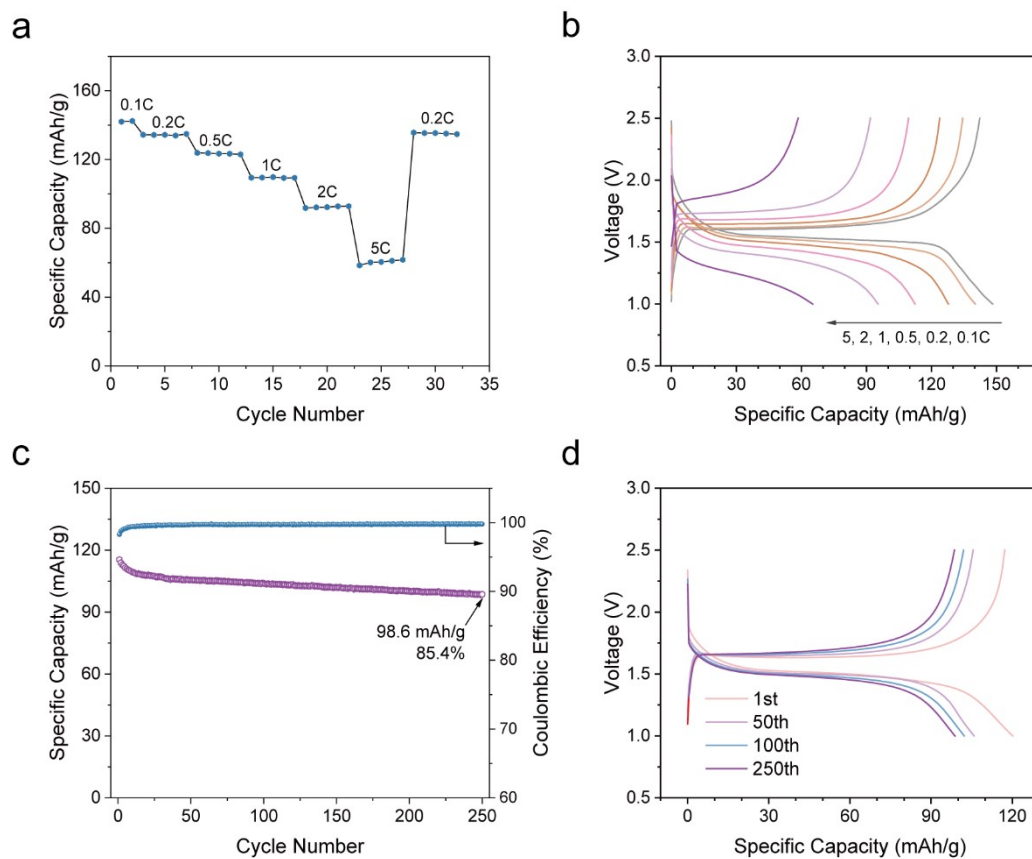


Figure S5. a,b) Rate capability and c,d) long-term charge/discharge curves of $\text{Li}_4\text{Ti}_5\text{O}_{12}$ half cells.

The rate capability and cycle performance of the upcycled LTO are also investigated. Noteworthy, the electrochemical performance of the as-prepared LTO material can be further improved by composition and structure optimizations, which is not the focus of this work.

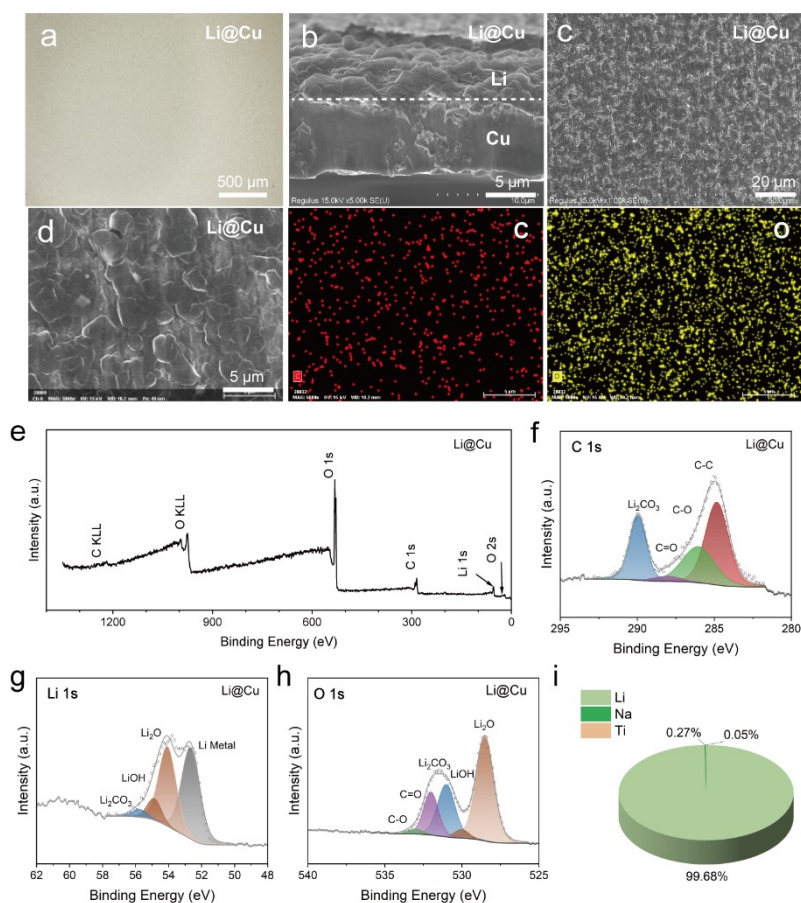


Figure S6. The surface morphology and composition of the as-prepared lithium metal film. a) The optical microscope image, b) cross-sectional SEM, c,d) top-view SEM and EDS mapping images of lithium metal film. e) The survey spectrum, f) C 1s, g) Li 1s and h) O 1s XPS spectra of lithium metal film. i) The ICP-OES analysis of lithium metal film from VTR process.

The EDS mapping images display uniformly distributed C and O elements from the inevitable reactions of lithium metal with the air. Only Li, C and O elements can be identified from the survey XPS spectrum. In the C 1s spectrum, besides the typical peaks from C-C, C-O and C=O bonds, a prominent peak at 290.0 eV refers to Li_2CO_3 . In the Li 1s and O 1s XPS spectra, Li_2O , LiOH and Li_2CO_3 can be identified at 54.1/54.9/55.8 eV and 528.5/530.0/531.0 eV, respectively⁴. The remaining deconvoluted peak at 52.7 eV in Li 1s spectrum can be assigned to the metallic lithium⁵. The purity of lithium metal is 99.68 mol% from ICP-OES analysis, 0.27 mol% of Na comes from sodium impurities in LiOH.

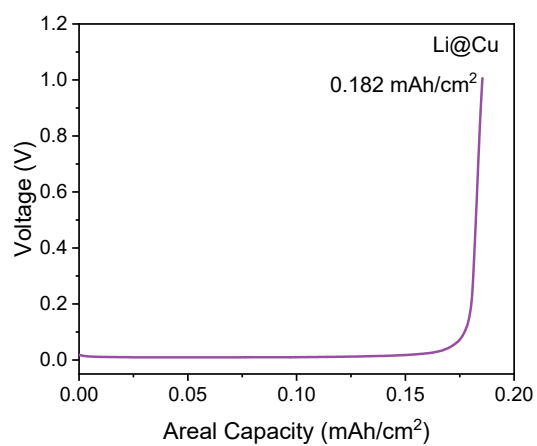


Figure S7. The initial charge curve of lithium metal film (0.9 μm in thickness measured by a quartz crystal sensor).

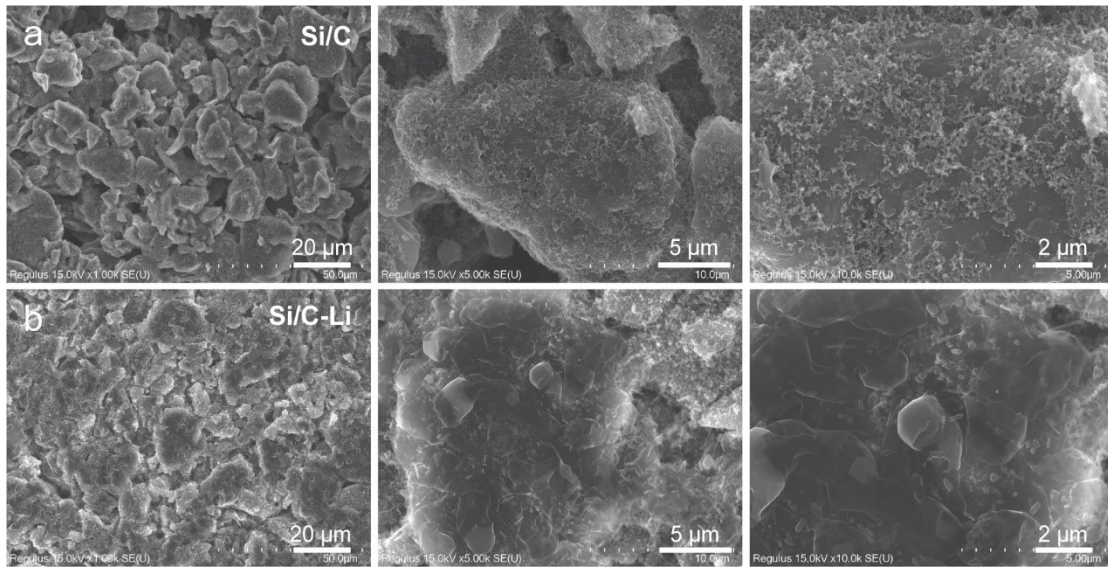


Figure S8. SEM images of a) Si/C and b) Si/C-Li electrodes.

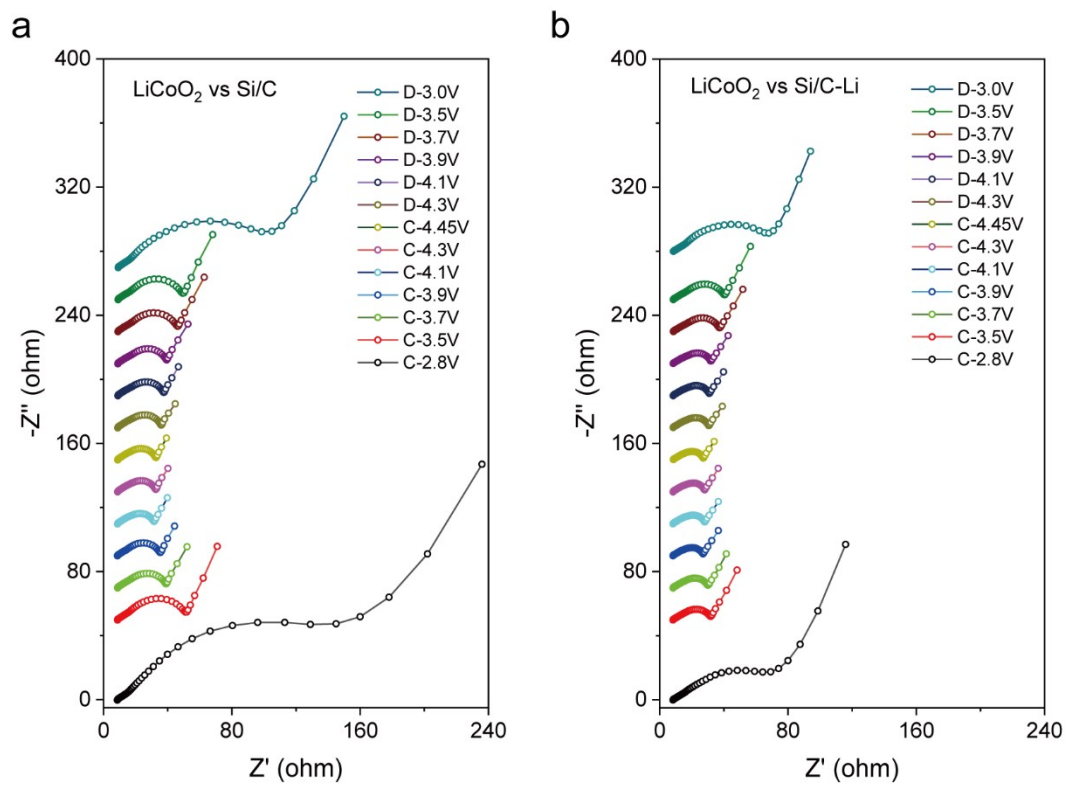


Figure S9. Electrochemical impedance spectroscopy (EIS) measurements of a) LiCoO₂ vs Si/C and b) LiCoO₂ vs Si/C-Li full cells.

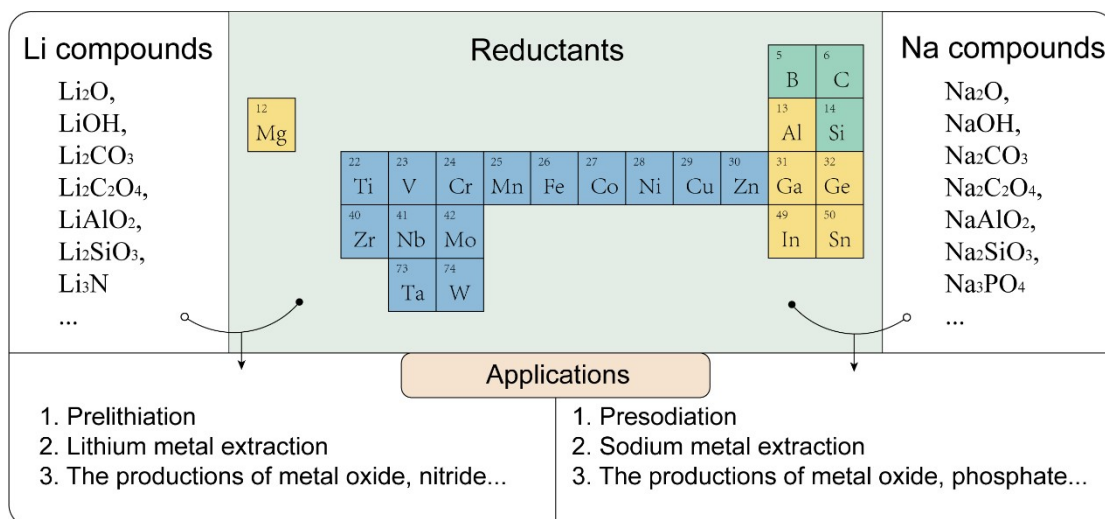


Figure S10. Future research directions and applications in lithium and sodium metals VTR.

Table S1. The cost and comprehensive unit price of vacuum thermal evaporation anode pre-lithiation method.

Material cost	The price of lithium ingot including transportation and storage (\$/kg)	707.3
	Lithium film thickness (μm)	1
	Lithium utilization rate	90%
	Lithium usage (kg/m^2)	5.93×10^{-4}
	Unit price ($\$/\text{m}^2$)	0.420
Electric cost	Electrode width (m)	0.6
	Electrode length (m)	4000
	Electrode travel speed (m/min)	15
	Pre-lithiation time (h)	4.44
	Equipment power consumption (kWh)	100
	Electricity price ($\$/\text{kWh}$)	0.207
	Unit price ($\$/\text{m}^2$)	0.038
Equipment cost	Cost of evaporation equipment (\$)	1.11×10^6
	Annual production capacity (m^2)	3.50×10^6
	Equipment depreciation time (year)	8
	Unit price ($\$/\text{m}^2$)	0.039
Comprehensive unit price ($\$/\text{m}^2$)		0.497

Table S2. The formation energy of stable metal oxides containing Li or Ti elements, reaction equation and corresponding thermodynamic enthalpy changes (ΔH_f) between Ti and Li_2O . The aforementioned thermodynamic data are garnered from the Materials Project³.

Formula	ΔH_f (eV/formula)	Reaction	ΔH_f (eV)
Li_2O	-6.186	-	-
Ti_6O	-6.419	$3\text{Ti} + 1/2 \text{Li}_2\text{O} = 1/2 \text{Ti}_6\text{O} + \text{Li}$	-0.116
Ti_3O	-6.280	$3/2 \text{Ti} + 1/2 \text{Li}_2\text{O} = 1/2 \text{Ti}_3\text{O} + \text{Li}$	-0.048
Ti_2O	-6.108	$\text{Ti} + 1/2 \text{Li}_2\text{O} = 1/2 \text{Ti}_2\text{O} + \text{Li}$	0.039
Li_4TiO_4	-24.372	$1/4 \text{Ti} + \text{Li}_2\text{O} = 1/4 \text{Li}_4\text{TiO}_4 + \text{Li}$	0.093
LiTiO_2	-11.920	$1/3 \text{Ti} + 2/3 \text{Li}_2\text{O} = 1/3 \text{LiTiO}_2 + \text{Li}$	0.151
Li_2TiO_3	-17.898	$1/4 \text{Ti} + 3/4 \text{Li}_2\text{O} = 1/4 \text{Li}_2\text{TiO}_3 + \text{Li}$	0.166
TiO	-5.818	$1/2 \text{Ti} + 1/2 \text{Li}_2\text{O} = 1/2 \text{TiO} + \text{Li}$	0.184
LiTi_2O_4	-22.729	$2/7 \text{Ti} + 4/7 \text{Li}_2\text{O} = 1/7 \text{LiTi}_2\text{O}_4 + \text{Li}$	0.289
$\text{Li}_7\text{Ti}_{11}\text{O}_{24}$	-135.576	$11/41 \text{Ti} + 24/41 \text{Li}_2\text{O} = 1/41 \text{Li}_7\text{Ti}_{11}\text{O}_{24} + \text{Li}$	0.314
Ti_2O_3	-16.520	$1/3 \text{Ti} + 1/2 \text{Li}_2\text{O} = 1/6 \text{Ti}_2\text{O}_3 + \text{Li}$	0.339
$\text{Li}_4\text{Ti}_5\text{O}_{12}$	-67.284	$1/4 \text{Ti} + 3/5 \text{Li}_2\text{O} = 1/20 \text{Li}_4\text{Ti}_5\text{O}_{12} + \text{Li}$	0.348
$\text{Li}_2\text{Ti}_3\text{O}_7$	-38.316	$1/4 \text{Ti} + 7/12 \text{Li}_2\text{O} = 1/12 \text{Li}_2\text{Ti}_3\text{O}_7 + \text{Li}$	0.378
Ti_3O_5	-27.048	$3/10 \text{Ti} + 1/2 \text{Li}_2\text{O} = 1/10 \text{Ti}_3\text{O}_5 + \text{Li}$	0.388
TiO_2	-10.506	$1/4 \text{Ti} + 1/2 \text{Li}_2\text{O} = 1/4 \text{TiO}_2 + \text{Li}$	0.466

Table S3. The total mass calculation of the LiCoO₂ vs Si/C full cell.

		mass (mg)	Total mass (mg)	Area (cm ²)
Anode	Si/C	8.772	42.201	1.539
	Super P	0.487		
	Sodium alginate	0.487		
	Cu foil	13.420		
Cathode	LiCoO ₂	12.667	42.201	1.131
	Super P	0.704		
	PVDF	0.704		
	Al foil	4.960		

Table S4. The energy density calculations of the full cells.

	Capacity (mAh)	Energy (mWh)	Total mass of anode and cathode (mg)	Energy density (Wh/kg)
LiCoO ₂ vs Si/C	2.009	7.721	42.201	183.0
LiCoO ₂ vs Si/C-Li	2.467	9.467	42.201	224.3

Table S5. Some recommendable thermal reduction reactions with low reaction enthalpies (Δ_rH). The thermodynamic data are garnered from the Materials Project³.

Reductants	Reactions	Products	Δ_rH (eV)
B	$1/3 \text{ B} + \text{Li}_2\text{O} = 1/3 \text{ Li}_3\text{BO}_3 + \text{Li}$	Li_3BO_3	0.222
Zr	$1/4 \text{ Zr} + 3/4 \text{ Li}_2\text{O} = 1/4 \text{ Li}_2\text{ZrO}_3 + \text{Li}$	Li_2ZrO_3	0.078
Ta	$1/5 \text{ Ta} + 4/5 \text{ Li}_2\text{O} = 1/5 \text{ Li}_3\text{TaO}_4 + \text{Li}$	Li_3TaO_4	0.386
Ti	$1/4 \text{ Ti} + 3/5 \text{ Na}_2\text{O} = 1/20 \text{ Na}_4\text{Ti}_5\text{O}_{12} + \text{Na}$	$\text{Na}_4\text{Ti}_5\text{O}_{12}$	-0.677
Mn	$1/3 \text{ Mn} + 2/3 \text{ Na}_2\text{O} = 1/3 \text{ NaMnO}_2 + \text{Na}$	NaMnO_2	0.060

It should be emphasized that reduction residues of Li_3BO_3 , Li_2ZrO_3 , Li_3TaO_4 (Table S5) can be used for the coating layer of the cathode materials to further improve their cycling performance, while $\text{Na}_4\text{Ti}_5\text{O}_{12}$ and NaMnO_2 can serve as the anode and cathode materials for sodium-ion battery.

References

- 1 T. H. Wan, M. Saccoccio, C. Chen and F. Ciucci, *Electrochim. Acta*, 2015, **184**, 483–499.
- 2 S. P. Ong, L. Wang, B. Kang and G. Ceder, *Chem. Mater.*, 2008, **20**, 1798–1807.
- 3 A. Jain, G. Hautier, S. P. Ong, C. J. Moore, C. C. Fischer, K. A. Persson and G. Ceder, *Phys. Rev. B - Condens. Matter Mater. Phys.*, 2011, **84**, 1–10.
- 4 K. N. Wood and G. Teeter, *ACS Appl. Energy Mater.*, 2018, **1**, 4493–4504.
- 5 K. Nagao, M. Suyama, A. Kato, C. Hotehama, M. Deguchi, A. Sakuda, A. Hayashi and M. Tatsumisago, *ACS Appl. Energy Mater.*, 2019, **2**, 3042–3048.